



www.sciencemag.org/cgi/content/full/science.1221976/DC1

Supplementary Materials for
**Membrane Fusion Intermediates via Directional and Full Assembly of
the SNARE Complex**

Javier M. Hernandez, Alexander Stein, Elmar Behrmann, Dietmar Riedel, Anna
Cypionka, Zohreh Farsi, Peter J. Walla, Stefan Raunser, Reinhard Jahn*

*To whom correspondence should be addressed. E-mail: rjahn@gwdg.de

Published 31 May 2012 on *Science* Express
DOI: 10.1126/science.1221976

This PDF file includes:

Materials and Methods
Supplementary Text
Figs. S1 to S9
Full References

Materials and Methods

Protein constructs

All proteins used in this study were derived from *Rattus norvegicus*. Constructs for full-length synaptobrevin 2 (amino acids 1-116), soluble synaptobrevin 2 (1-96) and a C-terminal fragment of synaptobrevin 2 (45-96, 49-96, 53-96) were cloned into pET28a vectors containing His₆ tags as described (7, 14, 31). The constituents of the Δ N complex were assembled using separately expressed constructs or were co-expressed. In the former, syntaxin 1A lacking the N-terminal Habc domain (183-288) and a cysteine-free variant of SNAP-25A were cloned into His₆-containing pET28a vectors (7, 32). In the latter, syntaxin 1A (183-288) and C-terminal synaptobrevin (49-96) were cloned together on a pETDuet-1 vector without a His₆-tag as previously described (33). Other constructs used in this study are described elsewhere and include full-length synaptotagmin (1-421) (33), cysteine-mutated synaptobrevin 1-96 on position 28 (34), and cysteine-mutated synaptobrevin 1-116 on position 28 (34). Cysteine-mutated synaptobrevin 49-96 on position 79 used for determining displacement kinetics from the Δ N complex was generated from a full-length synaptobrevin construct with appropriate primers and cloned onto a pET28a vector using restriction sites NdeI and XhoI.

Protein expression and purification.

Proteins were expressed in *E. coli* strain BL-21 (DE3) (Novagen) and purified according to previously published procedures (7, 33, 35). SNAREs or SNARE complexes were purified to near homogeneity with ion exchange chromatography on a Äkta system (GE Healthcare) essentially as described (35), the main difference being that buffers for ion exchange chromatography for proteins and complexes used for reconstitution in large liposomes included 34 mM n-octyl- β -D-glucopyranoside (OG, Glycon). Samples were snap-frozen with liquid nitrogen and stored at -80 °C until further use.

Assembly of the Δ N complex.

The Δ N complex was assembled either by co-expression of the constituent SNAREs (33) or by assembly of separately expressed monomers (7), the only difference being the use of OG (34 mM) in the ion exchange buffer. Alexa488-labeled Δ N complex was assembled using the latter method. We found no qualitative differences in the activity of the Δ N complex assembled by both procedures as assessed by lipid-mixing and synaptobrevin binding assays.

Preparation of large liposomes.

Liposomes consisted of phosphatidylcholine (PC), phosphatidylethanolamine (PE), phosphatidylserine (PS) (all extracts from bovine brain, Avanti Polar Lipids) and cholesterol (CH) (from sheep wool, Avanti Polar Lipids). Large unilamellar liposomes were prepared by reverse phase evaporation (36). Lipid stock solutions were prepared in 2:1 chloroform:methanol and kept at -20 °C in argon-purged sealed vials.

Lipid films of composition PC:PE:PS:CH with molar ratio 5:2:2:1 were mixed in a pear-shaped flask (100 mL) previously purged with argon and the solvent removed by a step-wise vacuum pressure decrease from 500 to 20 mbar on a rotatory evaporator set-up

(~30-40 min). The dried lipid film was re-dissolved in diethyl ether (1.5 mL) followed by addition of liposome buffer (20 mM HEPES, 150 mM KCl, 1 mM DTT or 0.1 mM TCEP, pH 7.4; 0.5 mL). The resulting two-phase mixture was dispersed by sonication (Branson Sonifier, fine tip, 50% duty cycle at minimum intensity, 3 x 45 s with cooling periods on ice). Removal of diethyl ether from the suspension was achieved by gradually lowering the vacuum pressure (~1 h) to approximately 150 mbar. During removal a gel phase was formed which coalesced into an aqueous suspension containing multi-lamellar liposomes. The suspension was collected and diluted with an appropriate volume of liposome buffer to make the total lipid concentration 8 mM. Liposomes were extruded (Mini-Extruder, Avanti Polar Lipids) using polycarbonate membranes (Avanti Polar Lipids) of pore size 0.4 and then 0.1 μm (21-25 passes each), giving unilamellar liposomes in the diameter range of 90-130 nm as confirmed by field-flow-fractionation coupled to multi angle laser light scattering (FFF-MALLS, Wyatt Technology Corporation). Approximately 10-20 % of lipids were lost during membrane extrusion as quantified by phosphate analysis (37).

For labeled liposomes, 1,2-dioleoyl-*sn*-glycero-3-phosphoethanolamine-N-(7-nitro-2-1,3-benzoxadiazol-4-yl), abbreviated NBD-PE, and 1,2-dioleoyl-*sn*-glycero-3-phosphoethanolamine-N-(lissamine rhodamine B sulfonyl), abbreviated RHO-PE, were included in the mix (1.5 % each, Avanti Polar Lipids), with a corresponding 3 % reduction of unlabeled PE. For liposome fusion experiments used for chemical reduction by dithionite, 1,2-dioleoyl-*sn*-glycero-3-phospho-L-serine-N-(7-nitro-2-1,3-benzoxadiazol-4-yl), abbreviated NBD-PS, was used instead of NBD-PE.

Reconstitution of SNARES into large liposomes.

Reconstitution of synaptobrevin, including its mutants, synaptotagmin and the ΔN complex into large liposomes was done by n-octyl- β -D-glucopyranoside (OG)-mediated reconstitution using a modified procedure from Rigaud and co-workers (38). Although we attempted to reconstitute SNAREs by the so-called direct method (see supporting text for a description of the various mechanisms and definition of the R-value), a scan of different R-values revealed properties of proteoliposomes which were more consistent with a mixed mechanism (fig S1) (38).

Appropriate amounts of protein and OG were mixed to extruded 100 nm liposomes with extra liposome buffer added to make the final total lipid concentration 4 mM. Unless noted otherwise, SNARE-liposomes (including fluorophore-labeled SNAREs) were prepared with a nominal lipid/protein ratio of 500:1. To take into account the loss of lipids during membrane extrusion (~20 % measured by phosphate analysis), we assumed the starting total lipid concentration of protein-free liposomes was 6 mM. To determine the concentration of OG to add, we used an R-value (assuming an OG critical micelle concentration of 17 mM) of ~1.5. The OG concentration present in the protein detergent solution was taken into account in the calculation, therefore, the exact amount of OG and buffer to add depended on the stock concentration of the purified protein, the desired lipid/protein ratio of the liposomes and the volume of proteoliposomes to be prepared (between 250 and 500 μL).

As soon as OG/protein/lipids were mixed, detergent was removed by overnight dialysis at room temperature in liposome buffer with SM-2 Bio-Beads (Bio Rad, 2 $\text{g}\cdot\text{L}^{-1}$) followed by a second dialysis (3-6 h) using Slide-A-Lyzer dialysis cassettes of molecular

weight cut-off of 2 kDa and 10 kDa, respectively (Thermo Scientific). The size distribution of all large proteoliposomes used in this study was measured by FFF-MALLS and considered to be an important quality control for SNARE-liposome preparation. Size distributions of proteoliposomes remained essentially unchanged after 11 days when stored on ice.

Reconstitution of SNAREs into small liposomes.

SNAREs were reconstituted according to the co-micellization method with detergent removed by size-exclusion chromatography on a SMART system (Amersham Biosciences) using a PC 3.2/10 Fast Desalting column (GE Healthcare) as described (7). The lipid composition of the lipid mixes was PC:PE:PS:CH combined in the molar ratio 5:2:2:1, while for labeled liposomes 1.5 % (n/n) 1,2-dioleoyl - sn - glycerol - 3 - phosphor - L - serine - N - (7 - nitro - 2 - 1,3 - benzoxadiazol - 4 - yl), or NBD-PS, and 1.5 % (n/n) 1,2-dioleoyl - sn - glycerol - 3 -phosphoethanolamine - N - (lissamine rhodamine B sulfonyl), or RHO-PE, was included in the lipid mixture with a corresponding reduction in PS and PE. For this protocol SNAREs that were purified in 1 % (w/v) CHAPS-containing buffer during ion exchange chromatography were used.

Liposome fusion.

Lipid-mixing kinetics was monitored with the use of lipid-conjugates consisting of the FRET pair Rhodamine (RHO) and Nitrobenzoxadiazole (NBD) (7, 33). Liposome fusion reactions were performed and measured in either a Fluorolog 3 (Model FL322) or a Fluoromax 2 spectrometer equipped with a magnetic stirrer and a temperature controller (Jobin Yvon). Data was acquired with the software provided by the manufacturer. Excitation and emission wavelengths were 460 nm and 538 nm, respectively, and unless otherwise stated, reactions were performed at 30 °C in cuvette volumes of 1.2 mL. Typically synaptobrevin was reconstituted in NBD/RHO-labeled liposomes, however, we observed no differences when it was reconstituted in unlabeled liposomes. Reactions were started by mixing SNARE-liposomes (10-20 µL each) in liposome buffer and were terminated by adding reduced Triton X-100 (Sigma, 0.02% (v/v)). Dequenching signals were normalized to the maximum fluorescence produced by detergent solubilization and lipid-mixing curves were plotted as a percentage of the maximum fluorescence. For control reactions, soluble synaptobrevin 1-96 (2-4 µM) was pre-incubated with labeled liposomes (~5 min) before initiation of fusion.

Liposome fusion for testing synaptotagmin role in fusion.

Full-length synaptobrevin (wild-type or $\Delta 84$) and synaptotagmin were co-reconstituted with OG into unlabeled large liposomes with lipid composition of PC:PE:PS:CH with ratio 60:20:10:10. ΔN complex was reconstituted in NBD-PS/RHO-PE labeled large liposomes containing L- α -phosphatidylinositol-4,5-bisphosphate (PIP₂, extract from porcine brain, Avanti Polar Lipids). The lipid composition was PC:PE:PS:CH:PIP₂:RHO-PE:NBD-PS with ratio 50:18.5:17.5:10:1:1.5:1.5. All other conditions are described in the figure legend.

Liposome co-flotation on a density gradient for insertion assessment.

SNARE liposomes (50 μL) were mixed with Nycodenz (Axis Shield, 80 %, 50 μL) in a centrifuge insert with a maximum capacity of 250 μL . A second Nycodenz layer (30 %, 50 μL) was gently applied followed by another layer of liposome buffer (50 μL). The density gradient was centrifuged with a Beckman TL-100 ultracentrifuge (TLS55 rotor, $1.97 \times 10^5 \text{ G}$, 4 $^\circ\text{C}$, 1.5 h). Upon completion, 20 μL aliquots were carefully taken from the top of the gradient and analyzed by SDS-PAGE or western blot.

Orientation assessment by proteolytic digestion.

Orientation assessment of SNAREs reconstituted on large liposomes was done essentially as described with minor modifications (14). The principle of assessment is based on the accessibility of membrane-inserted transmembrane proteins to a protein-cleaving enzyme. Proteins inserted with inside-out orientation are protected from degradation while proteins with correct right side-out are exposed to proteolytic degradation. By comparing the amount of cleaved protein to the protein content of an untreated sample, an estimate of the correctly orientated protein can be made.

Proteolytic digestion reactions were performed in 50 μL volumes in liposome buffer. For evaluation of synaptobrevin orientation, tetanus toxin light chain (expressed in pET28a vector and purified on a mono-Q column) was used, whereas trypsin (Sigma) was used for ΔN complex liposomes. Synaptobrevin liposomes (30 μL) were incubated with tetanus toxin light chain (11.2 μM) and ΔN complex liposomes were incubated with trypsin (Sigma, $0.1 \text{ mg}\cdot\text{mL}^{-1}$) at 37 $^\circ\text{C}$ for 2 h in the presence or absence of 0.3 % (w/v) Triton X-100 (Sigma). A control reaction with only liposome buffer instead of tetanus toxin or trypsin was also performed. Synaptobrevin-containing samples were analyzed with SDS-PAGE followed by visualization with Coomassie Blue staining, and ΔN complex-containing samples were analyzed by Western blot and detected with monoclonal antibody for SNAP-25 (Synaptic Systems, Cl 71.1).

Fluorescence anisotropy.

Fluorescence anisotropy of a fluorophore is a measure of the polarization of emission when excited with polarized light. When the rate of emission is comparable to the rate of the rotational diffusion of the fluorophore, anisotropy values change according to factors that alter their diffusional properties, such as an increase in viscosity. When fluorophores are chemically linked to a protein, fluorescence anisotropy reflect the local conformational motion of the labeled residue, and can be used to probe for changes such as complex formation or dissociation of a labeled protein (39).

Anisotropy measurements were carried out essentially as described (7) in a Fluorolog 3 (Model FL322, Jobin Yvon) with in-built polarizers. Data was collected with the manufacturer's software with the integration time set at 2 or 4 s. Excitation and emission wavelengths were set to 488 nm and 520 nm and G factors were re-measured for every set of experiments. Unless stated otherwise, all experiments were done in a total volume of 1.2 mL at 30 $^\circ\text{C}$, while measurements in detergent were done with 50 mM n-octyl- β -D-glucopyranoside. All SNAREs and SNARE complexes with the corresponding cysteine mutations used for anisotropy experiments were labeled with an Alexa Fluor 488 C5-maleimide derivative (Invitrogen, abbreviated xxAlexa488 or xxA488, where xx denotes the position of the labeled residue) according to previously

described procedures (7, 16). We make note that the trace of fig. 1E (lower panel) is the same shown in fig. S6A (black).

Field-flow-fractionation multi angle laser light scattering.

Size distributions of liposomes were determined by FFF-MALLS using an Eclipse 2 set-up as described for synaptic vesicles (Wyatt Technology Corporation) (40). Angle-dependent light scattering values were fitted with the coated sphere model using the manufacturer's Astra software (real refractive index = 1.33, coating refractive index = 1.45, and coating thickness = 4 nm). This model assumes liposomes are perfectly symmetrical spheres with a bilayer membrane thickness of 4 nm and refractive index 1.45. With this input the software calculates the relative number (N) of liposomes as a function of the geometric radius (r) defined by a coated sphere model. The function N(r) was exported from the software and plotted using the Origin software package (Optilab). The total area of the size distributions was arbitrarily normalized to 1.

Electron microscopy.

Electron microscopy of liposomes visualized with negative staining was done as described previously (33). Cryo electron microscopy was done either with controlled sample vitrification via plunge-freezing using Vitrobot™ and imaged as described (41) or using a JEOL JEM-3200FSC electron microscope at an acceleration voltage of 200 kV operated at liquid nitrogen temperature. For the latter case, liposome mixtures were applied to a freshly glow-discharged holey carbon grid (Quantifoil R2/1 copper 400 mesh) overlaid with a continuous carbon film. Grids were blotted manually in a chamber with 95 % humidity at room temperature using a Gatan Cryoplunge3. Blotting time was between 10 and 14 s and grids were stored in liquid nitrogen-gas phase until analysis. An in-column omega energy filter was used to improve the image contrast by zero-loss filtering (15 eV slit width). Images were taken at a magnification of 8.5×10^4 and recorded on a 8.192 x 8.192 pixel TemCam-F816 at a defocus of 2 μ m (TVIPS, Gauting, Germany).

SNARE-liposomes (5-10 μ L) were typically mixed in a reaction volume of 80-100 μ L at either 25 or 30 °C with shaking. Aliquots (5 μ L) were then taken from the reaction mixture and applied to the grid and plunge-frozen. For controls, excess soluble synaptobrevin 1-96 was included in the reaction medium (~50 μ M). For each condition tested we prepared triplicate samples.

Counting of liposome interactions observed by EM.

We counted liposomes which were clearly visible both inside and outside of the holes of the grid. For undocked (free) liposomes, we included only those liposomes that were entirely localized inside the field of view. For counting docked liposomes, we considered both loosely and tightly docked liposomes for which at least one of the docking partners was fully observable within the field of view. Liposomes engaged in multiple-docking interactions were only counted once while liposomes undergoing hemifusion were identified by the presence of an extended single bilayer and considered separately (i.e. hemifusion was not treated as a single entity). At least one of the hemifused liposomes had to be entirely localized in the field of view. For cases of a

liposome involved simultaneously in hemifusion and docking, the liposome was counted once for hemifusion and once for docking.

Dithionite reduction for determining inner leaflet lipid-mixing.

Synaptobrevin NBD-PS/RHO-PE labeled liposomes (10 μ L) were pre-incubated in the fluorescence cuvette (1.2 mL) with stirring until signal stabilization. A sodium dithionite stock solution (100 mM, Fluka) was prepared in cold liposome buffer and kept on ice immediately before use. We found that excess amounts of dithionite permeated through the membrane quenching inner leaflet NBD-PS and giving rise to an unstable signal. We therefore tested a range of dithionite concentrations before each set of experiments, with optimal concentrations found to be in the range 750-900 μ M. To ensure saturating amounts of dithionite were being used, we added melittin as described in fig. S5. After a \sim 30 min incubation period following dithionite reduction, Δ N complex liposomes were mixed and inner leaflet lipid-mixing measured exactly as described for total lipid-mixing. For each set of experiments, we checked for any signs of photo bleaching on both the total and inner leaflet lipid-mixing profiles.

To compare total and inner leaflet lipid-mixing traces, the measured inner leaflet lipid-mixing (F_{inner}) was normalized to the maximum fluorescence obtained by detergent solubilization of the total lipid-mixing trace ($F_{\text{total-max}}$) according to the expression:

$$\frac{F_{\text{inner}} - F_{\text{inner-init}}}{F_{\text{total-max}} - F_{\text{inner-init}}} \times 100$$

where $F_{\text{inner-init}}$ refers to the initial inner leaflet fluorescence.

To calculate the expected inner leaflet lipid-mixing assuming full fusion conditions, we utilized the fraction of labeled NBD-PS in the inner leaflet with respect to the total, which is readily obtained by comparing NBD-PS fluorescence before and after dithionite addition (see fig. S5A). This empirically established ratio has several advantages over a theoretically based estimation, since it considers the true distribution of the lipid-dye being measured and takes into account the effect of lipid flip-flop and the size variability of the entire liposome ensemble. The inner/total NBD-PS ratio varied between 0.41 and 0.46 according to each preparation and was multiplied to the measured total lipid-mixing curve to get the expected inner leaflet lipid-mixing trace.

Fluorescence cross-correlation spectroscopy.

Details of the FCCS set-up and principle can be found in (6). We briefly describe the methodology and idea behind the technique. FCCS is based on the detection of individual, docked or fused liposomes diffusing through the detector volume of a dual-detection fluorescence confocal set-up. SNAREs are first reconstituted into two populations of liposomes that are differentially labeled with a FRET pair of dyes. Simultaneous dual detection of fluorescence bursts observed in the detector volume corresponds either to the diffusion of a fused liposome or to a pair or group of docked liposomes, the signals of which are then said to be cross-correlated. Thus, the degree of cross-correlation is proportional to the number of docked and fused liposomes. Fusion can be further distinguished from docking by measuring changes in the fluorescence lifetime of the donor dye as a result of FRET after lipid-mixing. Subtraction of a

normalized cross-correlation signal from the FRET lifetime signal gives rise to a profile that reflects the evolution of docked liposomes.

Full-length synaptobrevin or synaptobrevin $\Delta 84$ was reconstituted in large liposomes containing Texas Red-PE (Molecular Probes, 1 % (n/n) total lipids) with a corresponding reduction in unlabeled PE, whereas ΔN complex was reconstituted in large liposomes containing Oregon Green-PE with a corresponding reduction in unlabeled PE (Molecular Probes, 1 % (n/n) total lipids). Lipid/protein ratio was 500:1 for all preparations. For fusion reactions, SNARE-liposomes were diluted (1:80) prior to mixing (30 °C) and measured as previously described (6). Controls were performed in the presence of excess soluble synaptobrevin (1-96) showing all observed liposome interactions were SNARE-mediated, however, they are not depicted in the figures for clarity. Solid lines in fig. 2G and 3B represent fits according the equations presented in fig. 6 of (6).

Supplementary Text

Protein reconstitution into large liposomes.

Two mechanistically distinct strategies have been described for reconstitution of transmembrane proteins. The co-micellization method (referred sometimes as the “standard” method owing to its widespread application) involves the dissolution of purified transmembrane proteins in a mixture of detergent and excess phospholipids, resulting in protein-detergent-phospholipid and detergent-phospholipid micelles. Initial removal of the detergent leads to the coalescence of both types of micelles, with further detergent depletion driving the protein to take part of the micellar-to-lamellar transition and spontaneously inserting into the forming bilayer. In the direct reconstitution method (also known as the “step-by-step” method) preformed liposomes are exposed to a critical amount of detergent followed by a micellar solution of protein (42). At appropriate conditions, progressive removal of detergent results in direct insertion of transmembrane protein into detergent-doped membrane bilayers. A third and hybrid mechanism at detergent concentrations intermediate of those needed for direct reconstitution and reconstitution via co-micellization is also observed and contains features from both mechanisms.

The mechanisms by which transmembrane proteins are reconstituted have been rationalized as part of a 3-stage model where the critical parameter is the relative amount of detergent above the critical micelle concentration (CMC) to the total lipid content. This ratio, denoted R, is formalized by the expression (38):

$$\frac{[D_{\text{total}} - D_{\text{cmc}}]}{[\text{lipid}]} = R$$

where $[D_{\text{total}}]$ and $[D_{\text{cmc}}]$ are the total detergent concentration and the CMC, respectively.

For reconstitution by co-micellization, excess amounts of detergent are used for total solubilization (i.e. high R-values) while in direct reconstitution only non-solubilizing amounts of detergent sufficient for saturating liposomes are added (i.e. low R-values, referred to as the onset of solubilization (43)). At detergent levels in between those

required for the onset and total solubilization, detergent micelles will partially and gradually solubilize liposomes and give rise to a two-phase system consisting of liposomes and micelles (called a “coexistence” phase (44)). Irrespective of which stage the lipid/detergent aggregates are found in, a key assumption and an integral part of the 3-stage reconstitution model is that liposome formation after detergent removal mirrors the opposite process that occurs during liposome solubilization (45). Thus, for any reconstitution system (lipid composition, detergent and protein) it is important to explore and characterize the reconstitution properties of proteoliposomes prepared at a range of different R-values.

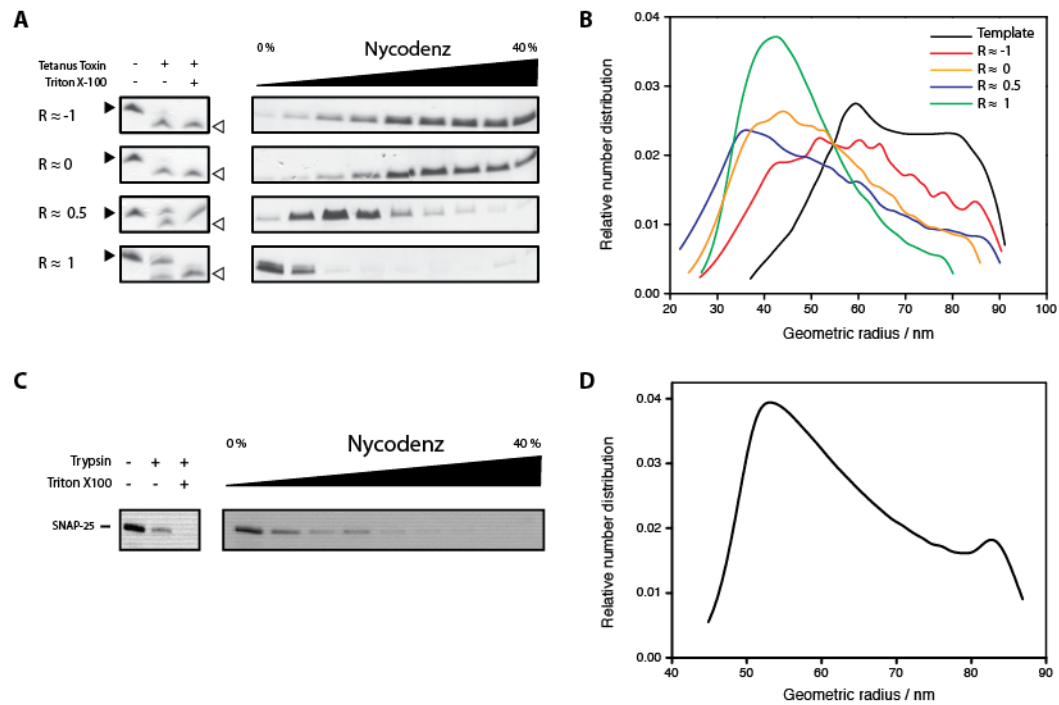


Fig. S1.

Characterization of n-octyl- β -D-glucopyranoside (OG)-mediated reconstitution of syb and Δ N complex into large liposomes. (A) Orientation and insertion efficiency of syb was critically dependent on the OG concentration defined by the R-value (see supporting text and methods for details). Left: syb/liposome mixtures (nominal lipid/protein (l/p) of 200:1) were incubated with OG at the indicated R-values followed by dialysis. Mixtures were treated with tetanus toxin in the absence or presence of Triton X-100 and analyzed by SDS-PAGE for protein orientation. Filled arrowheads indicate the position of intact syb while open arrowheads correspond to cleaved product (N-terminal part). Right: syb/liposome mixtures were separated by centrifugation on a Nycodenz gradient. Liposomes were observed in the top $\sim 40 \mu\text{L}$ and aliquoted fractions ($20 \mu\text{L}$) were analyzed by SDS-PAGE. Together these results suggest that syb is reconstituted with random orientation at high incorporation efficiency above $R \approx 1$. (B) Influence of the R-value on the size distributions of syb liposomes reconstituted with OG showing that size distributions were affected by the R-value relative to the original template distribution. The exact size distribution of a given SNARE liposome varied from preparation to preparation but radii distributions consistently peaked at $50 \pm 10 \text{ nm}$ when reconstituted at $R > 1$. Distributions were measured by FFF-MALLS and nominal l/p was 200:1 for all syb liposomes. (C) Left: orientation and insertion efficiency of Δ N complex reconstituted into large liposomes at $R \approx 1$. Δ N complex liposomes (nominal l/p of 200:1) were treated with trypsin in the absence or presence of Triton X-100 and analyzed by Western blot and detection of SNAP-25 (monoclonal antibody CL 71.1, Synaptic Systems). Right: Δ N complex liposomes were floated on a Nycodenz gradient, aliquoted ($20 \mu\text{L}$ fractions) and analyzed by Western blot and detection of SNAP-25. Liposomes were observed to float predominantly in the top $\sim 40 \mu\text{L}$ of the

gradient (from left). **(D)** Example of a size distribution of a ΔN complex liposome preparation measured by FFF-MALLS.

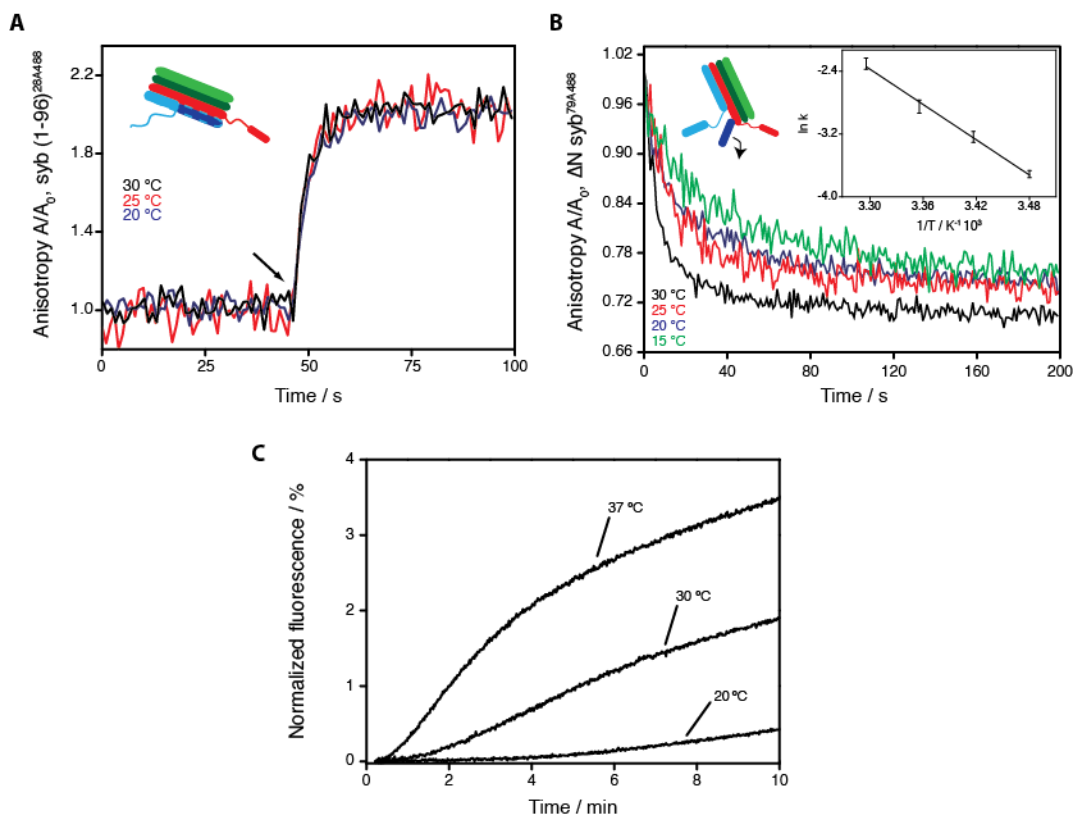


Fig. S2

Kinetic analysis of ΔN syb displacement from the ΔN complex reveals that displacement constitutes an additional energy barrier for SNARE complex assembly. (A) The effect of temperature on the bimolecular binding kinetics of syb to the ΔN complex monitored by anisotropy in detergent solution. ΔN complex (~ 400 nM) was added to soluble syb 1-96 labeled at position 28 with Alexa488 (syb 1-96^{28A488}, ~ 200 nM) at the indicated temperatures. The time of addition is marked by an arrow. The lack of effect of temperature on the reaction kinetics indicates the energy barrier for trans N-terminal binding is low. (B) Displacement kinetics of a ΔN complex labeled with an Alexa-488 dye on ΔN syb (ΔN syb 49-96^{79A488}) was measured in detergent solution by monitoring the decrease in fluorescence anisotropy (7). Displacement of ΔN syb 49-96^{79A488} from the ΔN complex (~ 200 nM) was started by addition of syb (in ~ 10 -fold excess) and was considerably slowed down by temperature. Inset: the finding that syb binding to the ΔN complex was temperature-insensitive allowed us to construct an Arrhenius plot for decay rate constants (k) of ΔN syb 49-96 displacement. Mono-exponential decay functions were fitted to displacement curves and the activation energy was found to be $56.6\text{--}77$ $\text{kJ}\cdot\text{mol}^{-1}$ (95% confidence interval). (C) Based on the high activation energy found for the displacement of ΔN syb 49-96, we hypothesized that lowering the reaction temperature should retard the displacement of ΔN syb 49-96 and delay the initiation of lipid-mixing. We tested this by measuring the lipid-mixing of large SNARE-liposomes, revealing that temperature had a pronounced effect on the lag phase and demonstrating that in addition to liposome size (fig. 1D) the displacement of the

ΔN sub-stabilizing fragment of the ΔN complex is a contributing kinetic factor to the lipid-mixing lag phase.

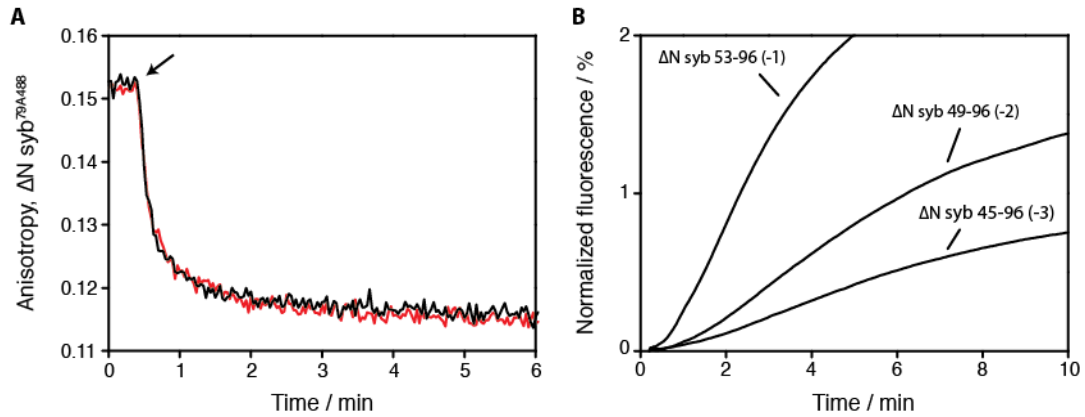


Fig. S3

The high activation energy for ΔN syb displacement originates from the disassembly of the N-terminal layers of ΔN syb and the fragment dissociates by the time an incoming syb assembles at the C-terminus of the SNARE complex. (A) Full-length syb (black) and syb $\Delta 84$ (red) (both at $\sim 2 \mu\text{M}$), containing a single deletion in position 84 which abolishes layer +8 of the SNARE complex, were added (arrow) to ΔN syb 49-96^{79A488} complex ($\sim 200 \text{ nM}$). Fluorescence anisotropy was measured and compared at 30°C , revealing no differences in their ability to displace the ΔN syb 49-96 fragment. Since syb $\Delta 84$ can only assemble correctly until layer +7 and given that it displaces ΔN syb 49-96 as readily as wild-type syb, we conclude that the zippering of syb $\Delta 84$ as it assembled at layer +7 was unimpeded and that ΔN syb 49-96 had already been removed from the ΔN complex. This deduction is in excellent agreement with a study showing that displacement of ΔN syb 49-96 occurs between layers -1 and +2 of the SNARE complex (fig. 2C in (46)). (B) We constructed ΔN complexes with ΔN syb fragments varying in only one layer of stabilization at the very N-terminus and reconstituted them in large liposomes to measure their lipid-mixing kinetics. As expected based on our previous analysis and on (46), we observed considerable changes in the lag phase, revealing that the origin of the high activation energy for displacement calculated in fig. S2 is most likely due to displacement of the first N-terminal layers. Based on this, we would expect that the rate of initial lipid-mixing shown for small liposomes in fig. 1D (solid line) would be even faster if we had used a ΔN complex stabilized by ΔN syb 53-96. Numbers in brackets denote the first layer of stabilization conferred by ΔN syb.

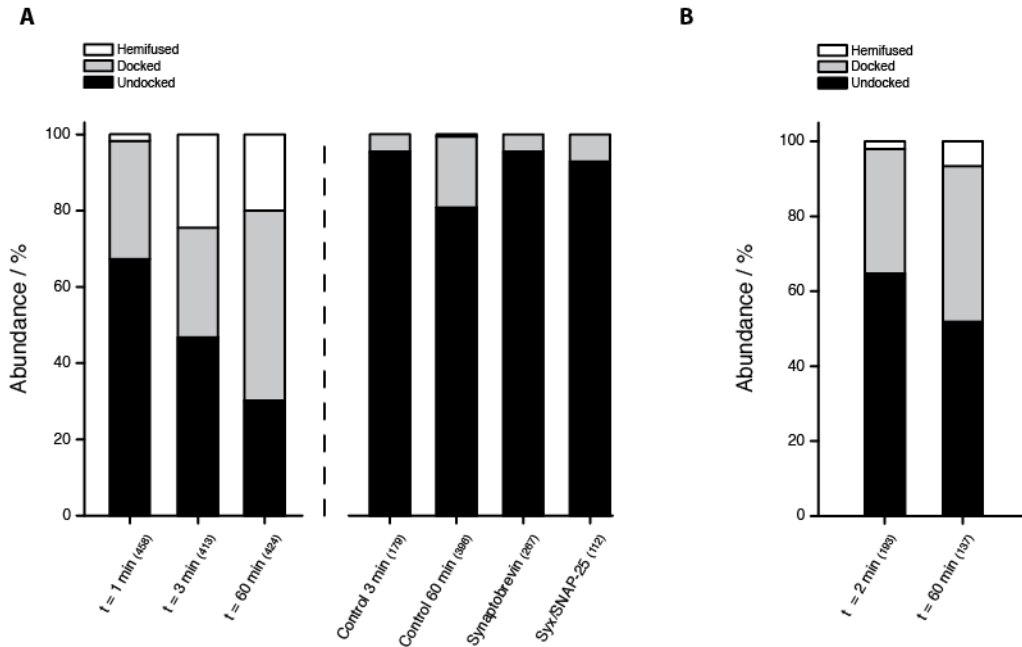


Fig. S4

Counting of docked and hemifused liposomes observed by cryo-EM and SNARE specificity of docking and hemifusion. (A) Syb and ΔN complex liposomes (nominal l/p = 500:1) were mixed and samples were plunge-frozen at 1, 3 and 60 min (left). The proportion of undocked (free), docked and hemifused liposomes were counted with the number of liposomes shown in brackets. Only liposomes that appeared to be in physical contact were classified as docked. By this criterion, both docking and hemifusion were SNARE-dependent as evidenced by controls where excess soluble syb 1-96 was added to the reaction medium or to unmixed syb or ΔN complex liposomes (right). (B) Counting of docking and hemifusion levels from a second experiment. Two more independent experiments were performed which exhibited initial and final docking and hemifusion levels intermediate between those depicted in (A) and (B). We stress that counting reveals only a qualitative evaluation of the presence of docking and hemifusion. The number of counted liposomes is depicted inside brackets.

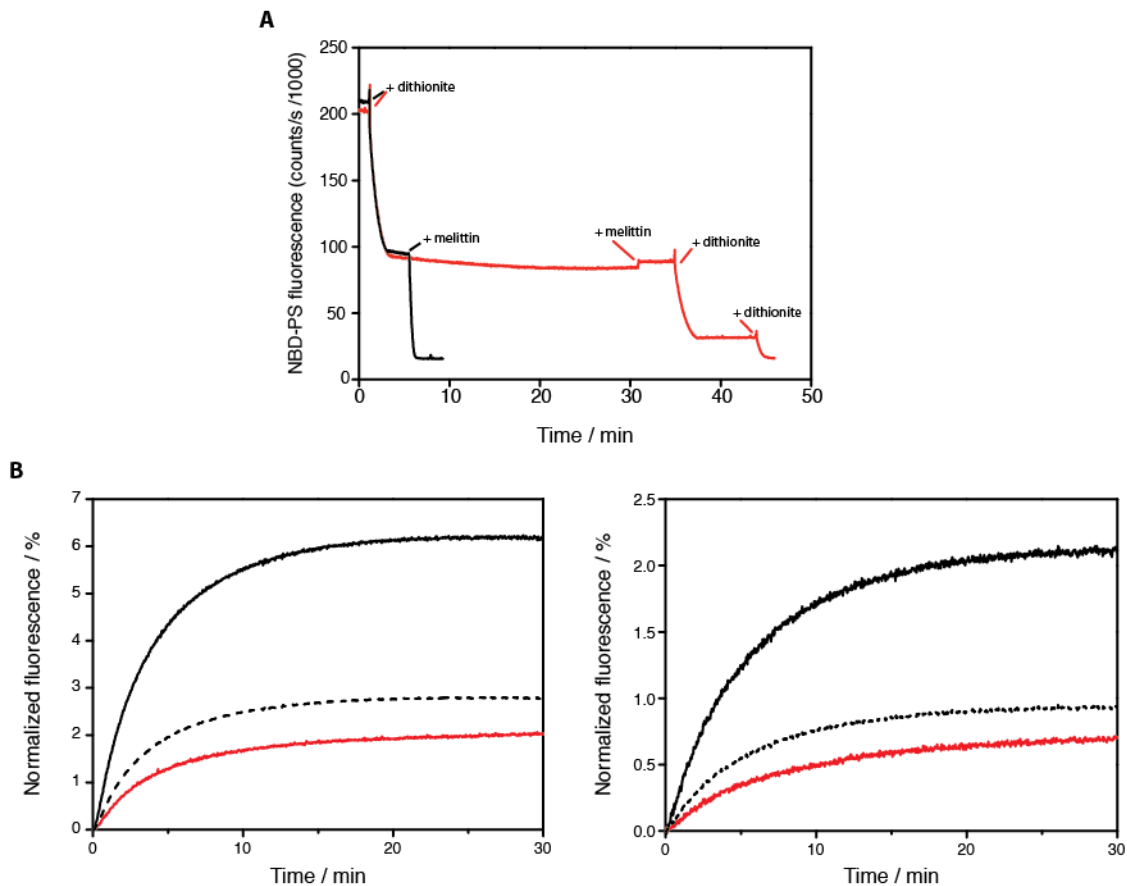


Fig. S5

Optimization of dithionite reduction of the outer monolayer NBD fluorescence on syb RHO-PE/NBD-PS liposomes for determination of inner-leaflet lipid-mixing and hemifusion is SNARE-density independent. (A) When externally applied, the reducing agent dithionite is commonly used to quench NBD fluorescence to reveal lipid-mixing in the inner leaflet, however, it is important to rule out the possibility that active dithionite may leak into the lumina during liposome fusion. Freshly-prepared dithionite (800 μM) was added to liposomes (total lipid concentration $\sim 60 \mu\text{M}$). After a ~ 3 min fluorescence stabilization period, the pore-forming peptide melittin ($\sim 1.8 \mu\text{M}$) was added at the indicated point (black curve). The formation of pores on the membrane bilayer by melittin causes dithionite to diffuse through to the lumen and quench NBD fluorescence on the inner leaflet monolayer, confirming that saturating levels of dithionite were used. However, if melittin is added after ~ 30 min, no signal quenching is observed (red curve), indicating that all dithionite is degraded, as previously reported (12). Additional dithionite was added to confirm melittin had formed pores. Based on this characterization, lipid-mixing experiments were performed ~ 30 min after dithionite addition to exclude any possibility of inner-leaflet NBD quenching as a result of inward dithionite leakage. (B) Hemifusion is not dependent on SNARE density. ΔN complex liposomes with nominal l/p = 500:1 (left) and l/p = 2000:1 (right) were mixed to syb liposomes (nominal l/p = 200:1) and their total (black) and inner leaflet lipid-mixing (red)

determined at 37 °C. Expected levels of inner leaflet lipid-mixing assuming full fusion conditions are shown as a dashed line. The observed/expected inner leaflet lipid-mixing ratio was comparable for both densities, suggesting the origin of hemifusion is related to an intrinsic property of SNARE function or to the energetics fusion pore opening in this system.

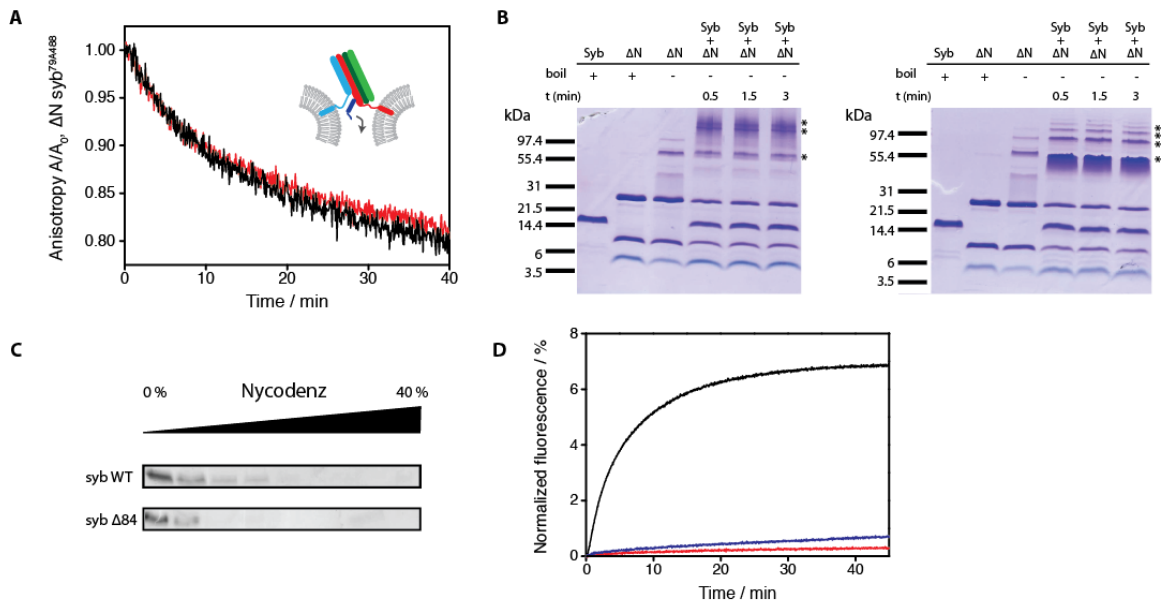


Fig S6

Syb wild-type and syb $\Delta 84$ have identical biochemical and reconstitution properties and doubling syb $\Delta 84$ density does not restore lipid-mixing to wild-type levels. (A) Large liposomes (20 μ L) containing ΔN syb 49-96^{79A488} complex were mixed with large liposomes containing wild-type syb (black) and syb $\Delta 84$ (red) and the fluorescence anisotropy measured, showing that ΔN syb displacement occurs at the same rate and that large liposomes are not arrested due to undisplaced ΔN syb. All liposomes had SNARE densities of nominal l/p = 500:1 and reactions were done at 30 °C. (B) Full-length syb $\Delta 84$ (right) forms SNARE complexes which are SDS-resistant, a hallmark of SNARE complex stability (47), as readily as full-length syb wild-type (left) as evaluated by SDS-PAGE in non-boiling conditions. Aliquots were taken from the reaction mixture and quenched on ice at three different time points, showing that the generation of SDS-resistant complexes (asterisks) was essentially completed within the first minute. Reactions consisted of a ΔN complex /syb ratio of 1:1.5 and were done at 37 °C in detergent solution. (C) Nycodenz co-floitation analysis of syb wild-type and syb $\Delta 84$ reconstituted in large liposomes showing that both are incorporated with comparable efficiency. Key: WT = wild-type; ΔN = ΔN complex. (D) ΔN complex liposomes (nominal 250:1) were mixed to wild-type syb (black) and syb $\Delta 84$ (red) liposomes both at nominal l/p = 500:1 at 37 °C. Doubling the density of syb $\Delta 84$ density to l/p = 250:1 (blue) has negligible effect on lipid-mixing and does not restore lipid-mixing to wild-type levels.

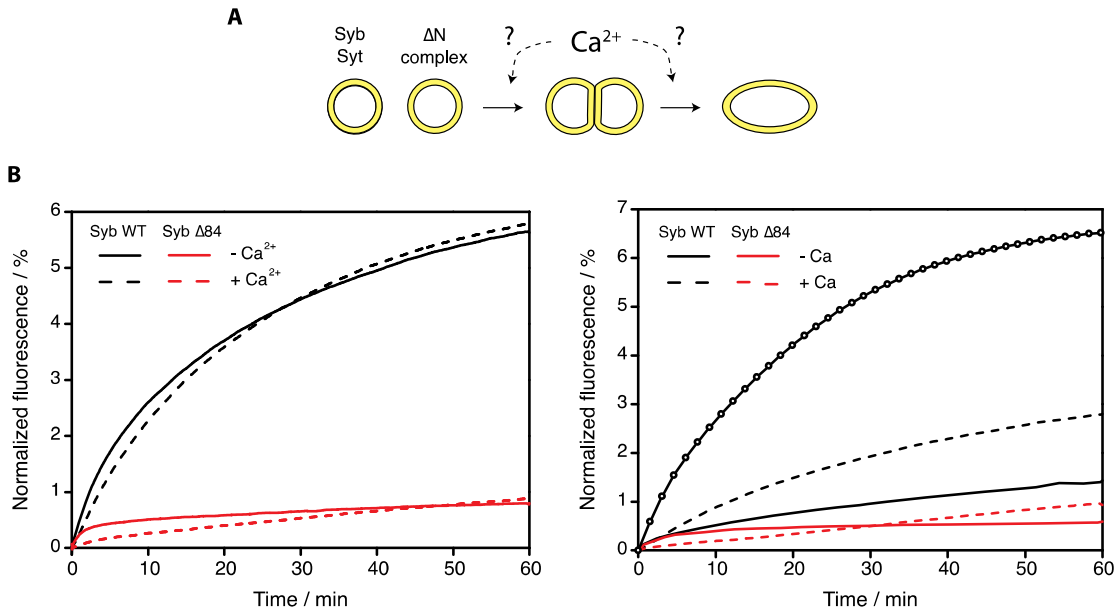


Fig. S7

The Ca²⁺ sensor synaptotagmin (syt) is unable to restore fusion from a tightly docked state mediated by syb Δ84. (A) The arrest of a trans SNARE complex that stabilizes a docked state allows testing of whether syt has an effect on fusion once bilayers are jointly apposed to each other. (B) Left: no effect of Ca²⁺ (500 μM) on the fusion of large liposomes co-reconstituted with full-length syt and wild-type syb or syb Δ84 at near physiological ionic strength (150 mM KCl). Right: no effect is seen on fusion on syb Δ84 liposomes at low ionic strength where electrostatic effects are unmasked (5 mM KCl, 300 mM sucrose). However, wild-type syb-mediated fusion is enhanced. We conclude syt does not assist in fusing membranes once they have been docked by a trans SNARE complex, but is consistent with a docking-promoting effect that operates before SNARE complex assembly. Basal fusion (open circles) corresponds to fusion at physiological ionic strength in the absence of Ca²⁺ and represents the maximum rate of lipid-mixing (20). SNAREs and syt were co-reconstituted each at nominal l/p = 1000:1 and reactions were performed at 30 °C. We note that reactions containing syt do not exhibit a pronounced lag phase, indicating syt either facilitates ΔN syb displacement and/or enhances liposome clustering which would prevent resolving the curvature-dependent delay for fusion initiation when looked at as an ensemble reaction.

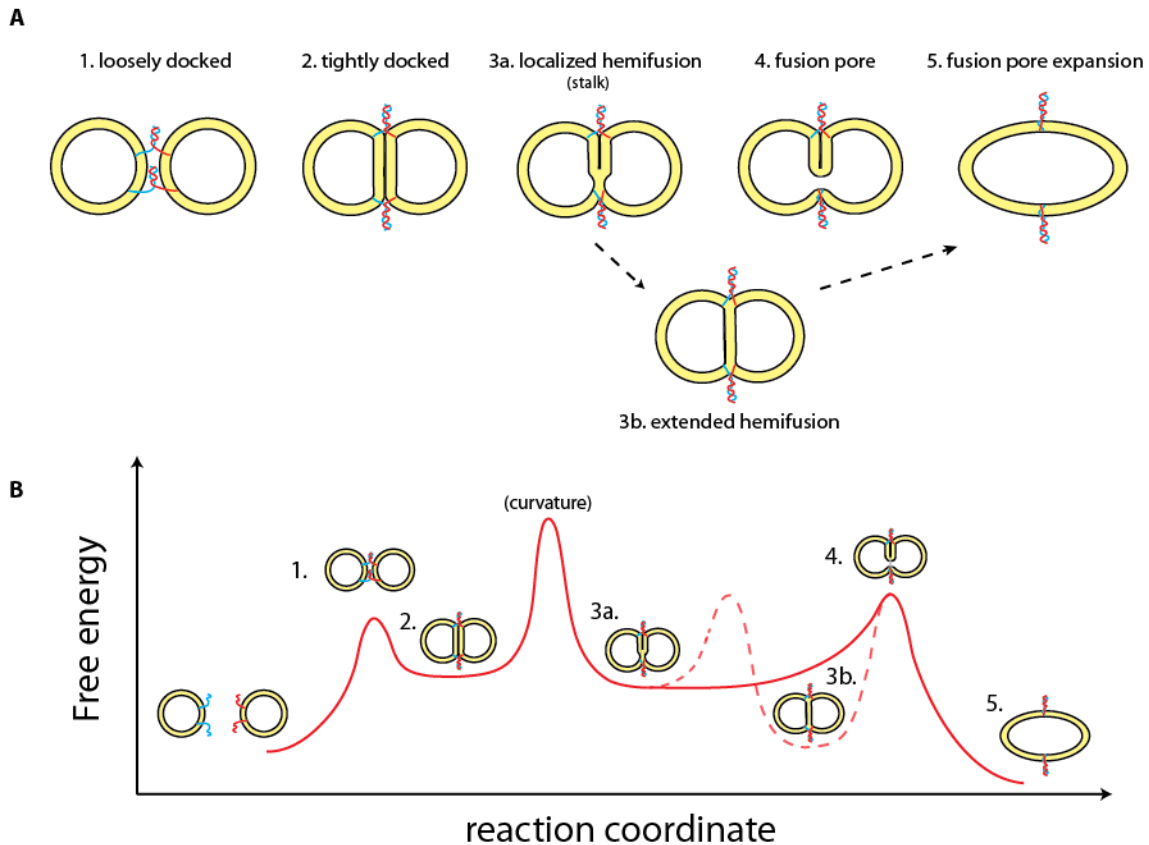


Fig. S9.

Model portraying the energetics and mechanics of SNARE-mediated fusion depicting the state of SNARE complex assembly and two metastable intermediate states identified in this work. (A) A reaction sequence for SNARE-mediated fusion. An initial loosely docked step (1) is mediated by trans N-terminal SNARE complex assembly. Further partial zippering brings opposing bilayers closer together into tight apposition (2), producing an extended docking zone with highly strained lipids that facilitates the formation of lipid stalks or splaying of lipid tails (3, 18). If enough pulling force is exerted, for instance by means of multiple SNARE complexes, full zippering of the core four-helix bundle and extended zippering of the linkers promotes merging of proximal leaflets at or near the edges, giving rise to an asymmetrical stalk-like structure which is a localized form of hemifusion (3a). Once formed, it may open a fusion pore (4) that then expands to complete fusion (5). However, we postulate that occasionally during assembly of TMDs a fusion pore does not form, expanding the diaphragm asymmetrically until proximal leaflets have merged completely and until the diaphragm has released a significant part of its tension (3b) (27). The syx:SN25 acceptor complex is represented as a single coil in the diagram for clarity.

The importance assigned here to the linkers connecting the SNARE motif with the TMD appears to be inconsistent with *in vivo* studies where insertion of 2 amino acids had no noticeable effect on fusion. However, the insertion was made directly adjacent to the TMD, which may not be as critical as disrupting the linker closer to the core of the SNARE complex as we have done here (48). Other *in vivo* studies appear to be

consistent with the involvement of the linkers in the force transmission mechanism of SNAREs (49, 50). In vitro, previous studies addressing the role of the linker in liposome fusion experiments (14, 51) may have missed its importance because small liposomes were used, which are much more fusion-prone due to curvature stress as shown in our study.

(B) The same sequence reaction shown in **(A)** but explained in the context of a possible energy landscape for SNARE-mediated fusion. To bring two bilayers into contact, SNAREs must overcome strong electrostatic and hydration forces, indicating that a high-energy transition state is present during this state (1). The electrostatic repulsion between bilayers taking part of the extended docking zone raises the energy of the system and so the tightly docked state is portrayed as lying on a local energy minimum of the coordinate (2). The effects of liposome size observed in this study suggest the ability for a tightly docked state to transit to the next intermediate state is curvature-dependent (indicated by the term “curvature” at a transition state with a high energy barrier). Initial merging of proximal leaflets leads to a stalk-like structure whose observation by x-ray diffraction suggests it minimizes the system energy (52) (3a). Since we have not seen this intermediate, we presume it is short-lived and that the activation energy of the next transition state it goes through is readily surmountable. We propose that from here there are two options. Either the diaphragm expands into an extended hemifusion state (3b), releasing its tension and lowering the system energy even further (dashed line), or it finds a more viable pathway by rupturing and opening a pore before it expands (4) and completing fusion (5) which appears to be a very fast process (53). The kinetically trapped extended hemifusion state may still be able to open a fusion pore, but its lower energy implicates that it must surpass a higher activation barrier to do so. It is plausible that specific lipids could lower the activation energy for fusion pore opening and thus make the extended hemifusion state a viable intermediate in vivo.

References

1. R. B. Sutton, D. Fasshauer, R. Jahn, A. T. Brunger, Crystal structure of a SNARE complex involved in synaptic exocytosis at 2.4 Å resolution. *Nature* **395**, 347 (1998).[doi:10.1038/26412](https://doi.org/10.1038/26412) [Medline](#)
2. T. Weber *et al.*, SNAREpins: minimal machinery for membrane fusion. *Cell* **92**, 759 (1998).[doi:10.1016/S0092-8674\(00\)81404-X](https://doi.org/10.1016/S0092-8674(00)81404-X) [Medline](#)
3. L. V. Chernomordik, M. M. Kozlov, Mechanics of membrane fusion. *Nat. Struct. Mol. Biol.* **15**, 675 (2008).[doi:10.1038/nsmb.1455](https://doi.org/10.1038/nsmb.1455) [Medline](#)
4. T. Y. Yoon, B. Okumus, F. Zhang, Y. K. Shin, T. Ha, Multiple intermediates in SNARE-induced membrane fusion. *Proc. Natl. Acad. Sci. U.S.A.* **103**, 19731 (2006).[doi:10.1073/pnas.0606032103](https://doi.org/10.1073/pnas.0606032103) [Medline](#)
5. M. L. Schwartz, A. J. Merz, Capture and release of partially zipped trans-SNARE complexes on intact organelles. *J. Cell Biol.* **185**, 535 (2009).[doi:10.1083/jcb.200811082](https://doi.org/10.1083/jcb.200811082) [Medline](#)
6. A. Cypionka *et al.*, Discrimination between docking and fusion of liposomes reconstituted with neuronal SNARE-proteins using FCS. *Proc. Natl. Acad. Sci. U.S.A.* **106**, 18575 (2009).[doi:10.1073/pnas.0906677106](https://doi.org/10.1073/pnas.0906677106) [Medline](#)
7. A. V. Pobbati, A. Stein, D. Fasshauer, N- to C-terminal SNARE complex assembly promotes rapid membrane fusion. *Science* **313**, 673 (2006).[doi:10.1126/science.1129486](https://doi.org/10.1126/science.1129486) [Medline](#)
8. V. S. Malinin, B. R. Lentz, Energetics of vesicle fusion intermediates: comparison of calculations with observed effects of osmotic and curvature stresses. *Biophys. J.* **86**, 2951 (2004).[doi:10.1016/S0006-3495\(04\)74346-5](https://doi.org/10.1016/S0006-3495(04)74346-5) [Medline](#)
9. J. Rizo, X. C. Chen, D. Araç, Unraveling the mechanisms of synaptotagmin and SNARE function in neurotransmitter release. *Trends Cell Biol.* **16**, 339 (2006).[doi:10.1016/j.tcb.2006.04.006](https://doi.org/10.1016/j.tcb.2006.04.006) [Medline](#)
10. Y. Xu, A. B. Seven, L. J. Su, Q. X. Jiang, J. Rizo, Membrane bridging and hemifusion by denatured Munc18. *PLoS ONE* **6**, e22012 (2011).[doi:10.1371/journal.pone.0022012](https://doi.org/10.1371/journal.pone.0022012) [Medline](#)
11. G. van den Bogaart *et al.*, One SNARE complex is sufficient for membrane fusion. *Nat. Struct. Mol. Biol.* **17**, 358 (2010).[doi:10.1038/nsmb.1748](https://doi.org/10.1038/nsmb.1748) [Medline](#)
12. J. Mima, C. M. Hickey, H. Xu, Y. Jun, W. Wickner, Reconstituted membrane fusion requires regulatory lipids, SNAREs and synergistic SNARE chaperones. *EMBO J.* **27**, 2031 (2008).[doi:10.1038/emboj.2008.139](https://doi.org/10.1038/emboj.2008.139) [Medline](#)
13. A. Bhalla, M. C. Chicka, W. C. Tucker, E. R. Chapman, Ca²⁺-synaptotagmin directly regulates t-SNARE function during reconstituted membrane fusion. *Nat. Struct. Mol. Biol.* **13**, 323 (2006).[doi:10.1038/nsmb1076](https://doi.org/10.1038/nsmb1076) [Medline](#)
14. T. J. Siddiqui *et al.*, Determinants of synaptobrevin regulation in membranes. *Mol. Biol. Cell* **18**, 2037 (2007).[doi:10.1091/mbc.E07-01-0049](https://doi.org/10.1091/mbc.E07-01-0049) [Medline](#)

15. A. M. Walter, K. Wiederhold, D. Bruns, D. Fasshauer, J. B. Sørensen, Synaptobrevin N-terminally bound to syntaxin-SNAP-25 defines the primed vesicle state in regulated exocytosis. *J. Cell Biol.* **188**, 401 (2010).[doi:10.1083/jcb.200907018](https://doi.org/10.1083/jcb.200907018) [Medline](#)
16. D. Fasshauer, M. Margittai, A transient N-terminal interaction of SNAP-25 and syntaxin nucleates SNARE assembly. *J. Biol. Chem.* **279**, 7613 (2004).[doi:10.1074/jbc.M312064200](https://doi.org/10.1074/jbc.M312064200) [Medline](#)
17. L. Wang, E. S. Seeley, W. Wickner, A. J. Merz, Vacuole fusion at a ring of vertex docking sites leaves membrane fragments within the organelle. *Cell* **108**, 357 (2002).[doi:10.1016/S0092-8674\(02\)00632-3](https://doi.org/10.1016/S0092-8674(02)00632-3) [Medline](#)
18. P. K. J. Kinnunen, J. M. Holopainen, Mechanisms of initiation of membrane fusion: role of lipids. *Biosci. Rep.* **20**, 465 (2000).[doi:10.1023/A:1010402819509](https://doi.org/10.1023/A:1010402819509) [Medline](#)
19. S. Martens, M. M. Kozlov, H. T. McMahon, How synaptotagmin promotes membrane fusion. *Science* **316**, 1205 (2007).[doi:10.1126/science.1142614](https://doi.org/10.1126/science.1142614) [Medline](#)
20. G. van den Bogaart *et al.*, Synaptotagmin-1 may be a distance regulator acting upstream of SNARE nucleation. *Nat. Struct. Mol. Biol.* **18**, 805 (2011).[doi:10.1038/nsmb.2061](https://doi.org/10.1038/nsmb.2061) [Medline](#)
21. A. Stein, G. Weber, M. C. Wahl, R. Jahn, Helical extension of the neuronal SNARE complex into the membrane. *Nature* **460**, 525 (2009). [Medline](#)
22. M. W. Hofmann *et al.*, Self-interaction of a SNARE transmembrane domain promotes the hemifusion-to-fusion transition. *J. Mol. Biol.* **364**, 1048 (2006).[doi:10.1016/j.jmb.2006.09.077](https://doi.org/10.1016/j.jmb.2006.09.077) [Medline](#)
23. Y. B. Xu, F. Zhang, Z. L. Su, J. A. McNew, Y. K. Shin, Hemifusion in SNARE-mediated membrane fusion. *Nat. Struct. Mol. Biol.* **12**, 417 (2005).[doi:10.1038/nsmb921](https://doi.org/10.1038/nsmb921) [Medline](#)
24. Y. Yang *et al.*, Dissection of SNARE-driven membrane fusion and neuroexocytosis by wedging small hydrophobic molecules into the SNARE zipper. *Proc. Natl. Acad. Sci. U.S.A.* **107**, 22145 (2010).[doi:10.1073/pnas.1006899108](https://doi.org/10.1073/pnas.1006899108) [Medline](#)
25. H. A. Scheidt, A. Pampel, L. Nissler, R. Gebhardt, D. Huster, Investigation of the membrane localization and distribution of flavonoids by high-resolution magic angle spinning NMR spectroscopy. *Biochim. Biophys. Acta* **1663**, 97 (2004).[doi:10.1016/j.bbamem.2004.02.004](https://doi.org/10.1016/j.bbamem.2004.02.004) [Medline](#)
26. J. L. Wong, D. E. Koppel, A. E. Cowan, G. M. Wessel, Membrane hemifusion is a stable intermediate of exocytosis. *Dev. Cell* **12**, 653 (2007).[doi:10.1016/j.devcel.2007.02.007](https://doi.org/10.1016/j.devcel.2007.02.007) [Medline](#)
27. A. Grafmüller, J. Shillcock, R. Lipowsky, The fusion of membranes and vesicles: pathway and energy barriers from dissipative particle dynamics. *Biophys. J.* **96**, 2658 (2009).[doi:10.1016/j.bpj.2008.11.073](https://doi.org/10.1016/j.bpj.2008.11.073) [Medline](#)

28. J. Nikolaus, M. Stöckl, D. Langosch, R. Volkmer, A. Herrmann, Direct visualization of large and protein-free hemifusion diaphragms. *Biophys. J.* **98**, 1192 (2010).[doi:10.1016/j.bpj.2009.11.042](https://doi.org/10.1016/j.bpj.2009.11.042) [Medline](#)
29. M. J. Stevens, J. H. Hoh, T. B. Woolf, Insights into the molecular mechanism of membrane fusion from simulation: evidence for the association of splayed tails. *Phys. Rev. Lett.* **91**, 188102 (2003).[doi:10.1103/PhysRevLett.91.188102](https://doi.org/10.1103/PhysRevLett.91.188102) [Medline](#)
30. H. J. Risselada, C. Kutzner, H. Grubmüller, Caught in the act: visualization of SNARE-mediated fusion events in molecular detail. *ChemBioChem* **12**, 1049 (2011).[doi:10.1002/cbic.201100020](https://doi.org/10.1002/cbic.201100020) [Medline](#)
31. D. Fasshauer, W. Antonin, M. Margittai, S. Pabst, R. Jahn, Mixed and non-cognate SNARE complexes. Characterization of assembly and biophysical properties. *J. Biol. Chem.* **274**, 15440 (1999).[doi:10.1074/jbc.274.22.15440](https://doi.org/10.1074/jbc.274.22.15440) [Medline](#)
32. M. Margittai, R. Langen, R. Jahn, SNARE-interactions in solution and in proteoliposomes studied by fluorescence spectroscopy and electron paramagnetic resonance (EPR). *Mol. Biol. Cell* **10**, 209A (1999).
33. A. Stein, A. Radhakrishnan, D. Riedel, D. Fasshauer, R. Jahn, Synaptotagmin activates membrane fusion through a Ca²⁺-dependent trans interaction with phospholipids. *Nat. Struct. Mol. Biol.* **14**, 904 (2007).[doi:10.1038/nsmb1305](https://doi.org/10.1038/nsmb1305) [Medline](#)
34. M. Margittai, D. Fasshauer, S. Pabst, R. Jahn, R. Langen, Homo- and heterooligomeric SNARE complexes studied by site-directed spin labeling. *J. Biol. Chem.* **276**, 13169 (2001).[doi:10.1074/jbc.M010653200](https://doi.org/10.1074/jbc.M010653200) [Medline](#)
35. C. G. Schuette *et al.*, Determinants of liposome fusion mediated by synaptic SNARE proteins. *Proc. Natl. Acad. Sci. U.S.A.* **101**, 2858 (2004).[doi:10.1073/pnas.0400044101](https://doi.org/10.1073/pnas.0400044101) [Medline](#)
36. N. Duzgunes, *Methods Enzymol.* **367**, 23 (2003).
37. G. Rouser, S. Fkeischer, A. Yamamoto, Two dimensional thin layer chromatographic separation of polar lipids and determination of phospholipids by phosphorus analysis of spots. *Lipids* **5**, 494 (1970).[doi:10.1007/BF02531316](https://doi.org/10.1007/BF02531316) [Medline](#)
38. J. L. Rigaud, D. Lévy, Reconstitution of membrane proteins into liposomes. *Methods Enzymol.* **372**, 65 (2003).[doi:10.1016/S0076-6879\(03\)72004-7](https://doi.org/10.1016/S0076-6879(03)72004-7) [Medline](#)
39. J. R. Lakowicz, *Principles of Fluorescence Spectroscopy* (Kluwer Academic/Plenum, New York, ed. 2, 1999)
40. S. Castorph *et al.*, Synaptic vesicles studied by dynamic light scattering. *Eur. Phys. J. E Soft Matter* **34**, 1 (2011).[doi:10.1140/epje/i2011-11063-2](https://doi.org/10.1140/epje/i2011-11063-2) [Medline](#)
41. M. Holt, D. Riedel, A. Stein, C. Schuette, R. Jahn, Synaptic vesicles are constitutively active fusion machines that function independently of Ca²⁺. *Curr. Biol.* **18**, 715 (2008).[doi:10.1016/j.cub.2008.04.069](https://doi.org/10.1016/j.cub.2008.04.069) [Medline](#)
42. D. Lévy, A. Gulik, A. Bluzat, J. L. Rigaud, Reconstitution of the sarcoplasmic reticulum Ca(2+)-ATPase: mechanisms of membrane protein insertion into

- liposomes during reconstitution procedures involving the use of detergents. *Biochim. Biophys. Acta* **1107**, 283 (1992).[doi:10.1016/0005-2736\(92\)90415-I](https://doi.org/10.1016/0005-2736(92)90415-I) [Medline](#)
43. D. Lichtenberg, R. J. Robson, E. A. Dennis, Solubilization of phospholipids by detergents. Structural and kinetic aspects. *Biochim. Biophys. Acta* **737**, 285 (1983). [Medline](#)
 44. O. López *et al.*, Octyl glucoside-mediated solubilization and reconstitution of liposomes: Structural and kinetic aspects. *J. Phys. Chem. B* **105**, 9879 (2001). [doi:10.1021/jp010273w](https://doi.org/10.1021/jp010273w)
 45. J. L. Rigaud, B. Pitard, D. Levy, Reconstitution of membrane proteins into liposomes: application to energy-transducing membrane proteins. *Biochim. Biophys. Acta* **1231**, 223 (1995).[doi:10.1016/0005-2728\(95\)00091-V](https://doi.org/10.1016/0005-2728(95)00091-V) [Medline](#)
 46. K. Wiederhold, D. Fasshauer, Is assembly of the SNARE complex enough to fuel membrane fusion? *J. Biol. Chem.* **284**, 13143 (2009).[doi:10.1074/jbc.M900703200](https://doi.org/10.1074/jbc.M900703200) [Medline](#)
 47. T. Hayashi *et al.*, Synaptic vesicle membrane fusion complex: action of clostridial neurotoxins on assembly. *EMBO J.* **13**, 5051 (1994). [Medline](#)
 48. J. Kesavan, M. Borisovska, D. Bruns, v-SNARE actions during Ca(2+)-triggered exocytosis. *Cell* **131**, 351 (2007).[doi:10.1016/j.cell.2007.09.025](https://doi.org/10.1016/j.cell.2007.09.025) [Medline](#)
 49. R. E. Guzman, Y. N. Schwarz, J. Rettig, D. Bruns, SNARE force synchronizes synaptic vesicle fusion and controls the kinetics of quantal synaptic transmission. *J. Neurosci.* **30**, 10272 (2010).[doi:10.1523/JNEUROSCI.1551-10.2010](https://doi.org/10.1523/JNEUROSCI.1551-10.2010) [Medline](#)
 50. M. Bretou, C. Anne, F. Darchen, A fast mode of membrane fusion dependent on tight SNARE zippering. *J. Neurosci.* **28**, 8470 (2008).[doi:10.1523/JNEUROSCI.0860-08.2008](https://doi.org/10.1523/JNEUROSCI.0860-08.2008) [Medline](#)
 51. J. A. McNew, T. Weber, D. M. Engelman, T. H. Söllner, J. E. Rothman, The length of the flexible SNAREpin juxtamembrane region is a critical determinant of SNARE-dependent fusion. *Mol. Cell* **4**, 415 (1999).[doi:10.1016/S1097-2765\(00\)80343-3](https://doi.org/10.1016/S1097-2765(00)80343-3) [Medline](#)
 52. L. Yang, H. W. Huang, Observation of a membrane fusion intermediate structure. *Science* **297**, 1877 (2002).[doi:10.1126/science.1074354](https://doi.org/10.1126/science.1074354) [Medline](#)
 53. C. K. Haluska *et al.*, Time scales of membrane fusion revealed by direct imaging of vesicle fusion with high temporal resolution. *Proc. Natl. Acad. Sci. U.S.A.* **103**, 15841 (2006).[doi:10.1073/pnas.0602766103](https://doi.org/10.1073/pnas.0602766103) [Medline](#)